Dark Spin-Cat States as Biased Qubits

Andreas Kruckenhauser,[1,2,3,*,‡] Ming Yuan,[4,*,†] Han Zheng,[4,*] Mikhail Mamaev,[4] Pei Zeng,[4] Xuanhui Mao,[4] Qian Xu,[4] Torsten V. Zache,[1,2] Liang Jiang,[4] Rick van Bijnen,[1,2,3] and Peter Zoller[1,2]

[1]*Institute for Theoretical Physics, University of Innsbruck, 6020 Innsbruck, Austria*

[2]*Institute for Quantum Optics and Quantum Information of the Austrian Academy of Sciences, 6020 Innsbruck, Austria*

[3]*PlanQC GmbH, 85748 Garching, Germany*

[4]*Pritzker School of Molecular Engineering, University of Chicago, Chicago, Illinois 60637, USA*

(Received 19 August 2024; revised 20 December 2024; accepted 15 May 2025; published 8 July 2025)

We present a biased atomic qubit, universally implementable across all atomic platforms, encoded as a "spin cat" within ground state Zeeman levels. The key characteristic of our configuration is the coupling of the ground state spin manifold of size $F_g \gg 1$ to an excited Zeeman spin manifold of size $F_e = F_g - 1$ using light. This coupling results in eigenstates of the driven atom that include exactly two dark states in the ground state manifold, which are decoupled from light and immune to spontaneous emission from the excited states. These dark states constitute the spin cat, leading to the designation "dark spin cat." We demonstrate that under strong Rabi drive and for large F_g, the dark spin cat is autonomously stabilized against common noise sources and encodes a qubit with significantly biased noise. Specifically, the bit-flip error rate decreases exponentially with F_g relative to the dephasing rate. We provide an analysis of dark spin cats and their robustness to noise, and we discuss bias-preserving single qubit and entangling gates, exemplified on a Rydberg tweezer platform.

DOI: 10.1103/w9zh-jwsx

Development of quantum computing hardware faces the requirements of scalability to large qubit numbers, while maintaining high levels of control and low error rates. To protect qubits from errors generated by imprecise control and environmental interactions, fault-tolerant quantum computing employs redundant encoding in logical qubits built from many physical qubits to detect and correct errors [1–6]. However, the large resource cost of fault-tolerant quantum computing poses a significant challenge for present quantum hardware. To mitigate this cost, one approach is to find different hardware-level encodings to suppress physical errors to higher order [7–9], introduce error bias [10–15], or detect leakage errors [16–18]. Encodings with strong error bias are particularly alluring, as they enable efficient quantum error correction (QEC) schemes with high permissible threshold for logical errors [12,19,20].

In light of remarkable advances with atomic quantum computing, including scaling to a large qubit count

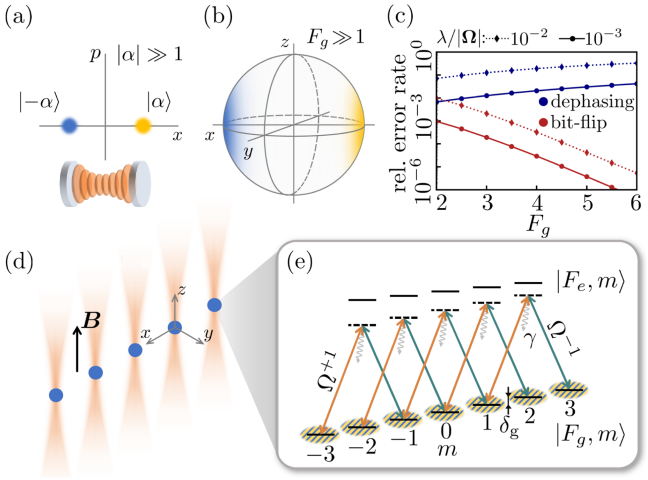

FIG. 1. Cat code: (a) phase space illustration of bosonic coherent states $|\pm\alpha\rangle$, with displacement $|\alpha| \gg 1$, realizing a cat code, with, e.g., photons in a cavity. (b) Wigner distribution of spin coherent states realizing a biased spin-cat code for $F_g \gg 1$. (c) Error rates due to colored noise with correlation time $1/\lambda$, relative to noise strength, are highly biased (bit-flip error decreases exponentially with F_g, while dephasing error only increases polynomially) and suppressed by increasing the laser Rabi frequency Ω. (d) Spin-cat codes are realizable with atomic platforms, (e) by coupling Zeeman-split spin manifolds with circularly polarized light Ω^q ($q = \pm 1$). The spin coherent states of (b) are DSs in the F_g manifold and distributed balanced over the magnetic sublevels m (mixed blue/yellow coloring), giving rise to a biased error model.

*These authors contributed equally to this work.

†Contact author: yuanming@uchicago.edu

‡Contact author: andreas.kruckenhauser@planqc.eu

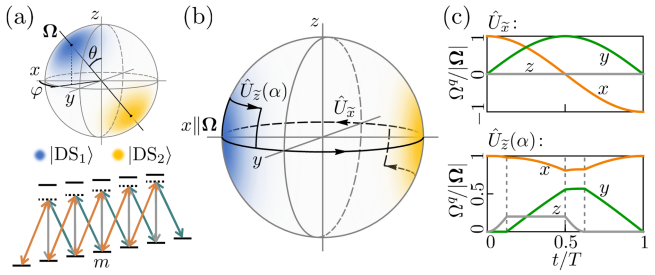

FIG. 2. (a) Wigner distribution of orthogonal dark spin-cat states on the Bloch sphere and associated light coupling scheme. (b) Dark spin-cat states on the equatorial plane and visualization of adiabatic single qubit gate trajectories. The associated parameter variations are displayed in panel (c), with T denoting the gate time.

[21–25], high fidelity gates [26–36], and early fault-tolerant quantum computation [37,38], we describe below a robust and biased qubit implementable across all atomic platforms. In analogy to the bosonic cat code, we consider encoding a qubit as a "spin cat" in a Zeeman F_g manifold $|F_g, m\rangle$, with $m = -F_g, \ldots, +F_g$, e.g., in a long-lived (hyperfine) spin manifold of states (see Fig. 1). While Ref. [39] discussed spin-cat encoding for "bare" Zeeman levels, the defining feature of the present setup is that we couple the ground state manifold F_g to an excited manifold $F_e = F_g - 1$ with light so that the eigenstates of the driven atom contain exactly two dark states (DSs) in the F_g manifold decoupled from light and unaffected by spontaneous emission from the excited states. We identify these DSs with the spin cat, hence the name "dark spin cat." In contrast to Refs. [40–44], we are interested in the limit of large F_g. For strong Rabi drive and large F_g, the dark spin cat will be shown to be robust and autonomously stabilized against typical noise sources and encode a qubit with highly biased noise. In particular, the bit-flip error rate is suppressed exponentially in F_g as compared to the dephasing rate; Fig. 1(c) shows a characteristic example of qubit robustness to "colored" noise. Below we discuss the unique noise resilience of dark spin cats, bias-preserving (BP) single qubit gates, and an illustration of entangling gates for the Rydberg (Ry) tweezer platform.

System—The atomic system we have in mind is illustrated in Figs. 1(d) and 1(e). We consider two hyperfine (HF) manifolds $|F_g, m\rangle$, $|F_e, m\rangle$ with an overall energy splitting ω_{eg}, dipole coupled by a laser or microwave radiation [45]. A static magnetic field $\mathbf{B}$ (defining the quantization axis) generates a Zeeman splitting $\delta_{g,e} = g_{g,e}\mu_B|\mathbf{B}|$, where $g_{g,e}$ denote the manifolds' Landé g factors and μ_B the Bohr magneton. We consider atoms with a large (nuclear) spin ($F_{g,e} \gg 1$) such as alkali or alkaline-Earth atoms or ions, and light fields with polarization $q \in \{0, \pm 1\}$, oscillation frequency ω_q, and Rabi frequency Ω^q fulfilling the Raman resonance criteria $\omega_q - \omega_{q'} = \delta_g(q - q')$.

In a rotating frame defined by the transformation $\hat{\mathcal{U}} = \exp\{i[\omega_0 \hat{P}_e + \delta_g(\hat{F}_{e,z} + \hat{F}_{g,z})]t\}$, the system Hamiltonian is

$$\hat{H}_{\mathrm{DS}}/\hbar = -\Delta \hat{P}_e - \delta \hat{F}_{e,z} + \frac{1}{2}\sum_{q=0,\pm 1}(\Omega^q \hat{\mathcal{C}}_q + \mathrm{H.c.}). \quad (1)$$

Here $\hat{F}_{g(e),i}$, with $i \in \{x, y, z\}$, are spin operators, $\hat{P}_e = \sum_m |F_e, m\rangle\langle F_e, m|$, while $\Delta = \omega_0 - \omega_{eg}$ denotes the overall detuning from the F_e states, and $\delta = \delta_g - \delta_e$ the differential Zeeman splitting. The light coupling is described by the operator $\hat{\mathcal{C}}_q = \sum_m \mathcal{C}^{F_e, m+q}_{F_g, m; 1, q} |F_e, m+q\rangle\langle F_g, m|$, with $\mathcal{C}^{F_e, m+q}_{F_g, m; 1, q}$ the Clebsch-Gordan (CG) coefficients incorporating dipole selection rules; see Supplemental Material [46]. Within the Wigner-Weisskopf approximation, spontaneous emission [47] from the F_e states with rate γ can be included as $-\Delta \to -\Delta - i\gamma/2$.

Dark states—For the case of $F_e = F_g - 1$ there are exactly two DSs, labeled $|\mathrm{DS}_{1,2}\rangle$, fulfilling $\hat{H}_{\mathrm{DS}}|\mathrm{DS}_{1,2}\rangle = 0$ [48]. The two DSs are fully located in the F_g manifold, thus immune to spontaneous emission, and are below identified as our qubit states. The DSs are up to an orthonormalization given by two spin coherent states (SCSs) $|\theta_{1,2}, \varphi_{1,2}\rangle = \exp(-i\varphi_{1,2}\hat{F}_{g,z})\exp(-i\theta_{1,2}\hat{F}_{g,y})|F_g, F_g\rangle$. The pairs of angles $(\theta_{1,2}, \varphi_{1,2})$ are determined by the two relative phases and amplitudes of the Rabi frequencies Ω^q. The two SCS are orthogonal, i.e., on opposite sides of the Bloch sphere $(\theta_2, \varphi_2) = (\pi - \theta_1, \pi + \varphi_1)$, if the Rabi frequency's Cartesian components $\Omega^x = (\Omega^{-1} - \Omega^{+1})/\sqrt{2}$, $\Omega^y = i(\Omega^{-1} + \Omega^{+1})/\sqrt{2}$ and $\Omega^z = \Omega^0$ are up to a global phase real valued in the rotating frame defined by $\hat{\mathcal{U}}$. In this case, θ_1 and φ_1 are given by the polar and azimuthal angle of $\mathbf{\Omega} = (\Omega^x, \Omega^y, \Omega^z)$, respectively; see Fig. 2(a) and Supplemental Material [46].

We now identify our dark spin-cat qubit with two SCSs pointing along the $\pm x$ axis,

$$\begin{aligned} |\tilde{0}\rangle &\equiv e^{-i\frac{\pi}{2}\hat{F}_{g,y}}|F_g, F_g\rangle = |\pi/2, 0\rangle, \\ |\tilde{1}\rangle &\equiv e^{-i\frac{\pi}{2}\hat{F}_{g,y}}|F_g, -F_g\rangle = e^{-i\pi F_g}|\pi/2, \pi\rangle; \end{aligned} \quad (2)$$

see Fig. 1(b). The qubit states $|\tilde{0}\rangle$ and $|\tilde{1}\rangle$ are DSs when $\Omega^y, \Omega^z = 0$ and are identical to the maximally stretched spin states along the x axis. The DS subspace is unaffected by laser intensity and phase fluctuations when the drives originate from the same source. States and operators labeled by $\tilde{\cdot}$ are associated with the logical qubit states hereafter.

A well-chosen adiabatic variation of laser parameters enables transporting the qubit states along trajectories on the Bloch sphere, with the two states always remaining antipodal. This allows for the implementation of a set of gates required for universal fault-tolerant quantum computation [11], where any errors will predominantly lead to

dephasing (as discussed in detail below). Bit-flip errors are instead exponentially suppressed by the spin length F_g, if the states are antipodal. In Figs. 2(b) and 2(c) we show the time-dependent $\mathbf{\Omega}(t)$ sweeps and the corresponding F_g Bloch sphere trajectories for a rotation around the $\tilde{z}$ axis $\hat{U}_{\tilde{z}}(\alpha) = \exp(-i\hat{\sigma}_{\tilde{z}}\alpha/2)$ by an angle α, and a π rotation around the $\tilde{x}$ axis $\hat{U}_{\tilde{x}} = \exp(-i\hat{\sigma}_{\tilde{x}}\pi/2)$. Here, $\hat{\sigma}_{\tilde{x}} = |\tilde{1}\rangle\langle\tilde{0}| + \text{H.c.}$, $\hat{\sigma}_{\tilde{y}} = -i(|\tilde{1}\rangle\langle\tilde{0}| - \text{H.c.})$ and $\hat{\sigma}_{\tilde{z}} = |\tilde{1}\rangle\langle\tilde{1}| - |\tilde{0}\rangle\langle\tilde{0}|$ are the dark spin-cat Pauli operators; thus, $\tilde{x}$, $\tilde{y}$, and $\tilde{z}$ refer to the logical qubit Bloch sphere axes. The implementation of $\hat{U}_{\tilde{z}}(\alpha)$ is based on holonomic quantum processes [49–52], with the enclosed area of the loop on the Bloch sphere determining the angle α.

Error analysis—Dominant external sources of noise for our system include fluctuating magnetic (electric) fields, laser intensity and phase fluctuations [53], and nonmagic trapping conditions for neutral atom quantum processors [54,55]. These sources of errors are described in the laboratory frame by low powers of spin operators $\prod_{i=x,y,z}(\hat{F}_{g,i})^{n_i}$ and typically $\sum_i n_i \leq 2$ [39]. When transformed into the rotating frame defined by $\hat{\mathcal{U}}$, any off-diagonal elements of such noise operators acquire time-oscillating prefactors with frequency δ_g and can, hence, be suppressed by an external magnetic field $\mathbf{B} \propto \delta_g$ [56]. Together with the observation that diabatic effects during gate operation manifest also as $\hat{F}_{g,z}$ (in a suitably chosen frame, see Supplemental Material [46]), this leaves longitudinal fields $\sim(\hat{F}_{g,z})^{n_z}$ as the main remaining source of noise in the rotating frame [41]. In the following we show that colored noise processes coupling to $\hat{F}_{g,z}$ with a strength and spectral width smaller than $|\mathbf{\Omega}|$ lead to a reduced and biased error model in the limit $F_g \gg 1$. Furthermore, if the states $|F_e, m\rangle$ are subject to spontaneous emission, the dark spin cat is also autonomously stabilized.

We first analyze the potential for longitudinal field perturbations ($2F_g - n_z \gg 1$) to cause bit-flip errors, which will *a priori* only occur when the two SCSs are not perfectly orthogonal, as, e.g., due to imperfect laser control. For the case of a small error ϵ in the angles $\theta_{1,2}, \varphi_{1,2}$, the off-diagonal matrix elements of perturbations $(\hat{F}_{g,z})^{n_z}$ are exponentially suppressed in F_g,

$$|\langle\theta_1,\varphi_1|(\hat{F}_{g,z})^{n_z}|\theta_2,\varphi_2\rangle| = |\epsilon|^{2F_g-n_z} 2^{-2F_g} \frac{(2F_g)!}{(2F_g-n_z)!} |\sin(\theta_1)|^k + \mathcal{O}(F_g^{n_z}\epsilon^{2F_g+1-n_z}). \tag{3}$$

Here, $k = n_z$ for $(\theta_2,\varphi_2) = (\pi - \theta_1 + \epsilon, \pi + \varphi_1)$ and $k = 2F_g$ for $(\theta_2,\varphi_2) = (\pi - \theta_1, \pi + \varphi_1 + \epsilon)$. This exponential suppression of bit-flip transitions is the basic building block of the biased error model.

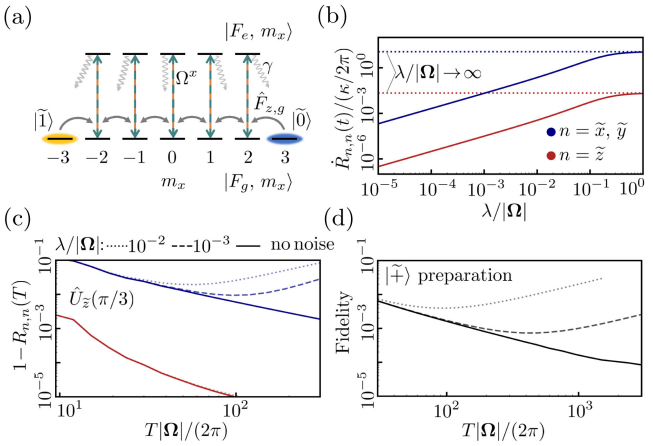

FIG. 3. (a) Autonomous stabilization: laser coupling ($F_g = 3$) in the rotated coordinate system with quantization axis $\mathbf{\Omega} = (\Omega^x, 0, 0)^T$. Note that $\Delta = \delta = 0$ and $|F_{g/e}, m_x\rangle$ are the eigenstates of $\hat{F}_{x,g/e}$. A noise process $\hat{F}_{z,g}$ couples states $|F_g, m_x\rangle$ adjacent in m_x. Decay of $|F_e, m_x\rangle$ is due to the CG coefficients directed "toward" the closest DS, as illustrated by wavy arrows indicating the average m_x change. (b) Time derivative of the diagonal elements of the PTM $\mathbf{R}(t)$ (effective error rates) for different values of $\lambda/|\mathbf{\Omega}|$. The time derivative is taken in the linear regime $t\kappa/(2\pi) \sim 1$. This and the remaining panels all share $\Delta = \delta = 0$, $|\mathbf{\Omega}|/\gamma = 2\pi$, $F_g = 4$, $\kappa = 10^{-4}|\mathbf{\Omega}|$, and $N_X = 3$. Panel (c) displays the error channels for $\hat{U}_{\tilde{z}}(\alpha = \pi/3)$, and (d) shows the state $|\widetilde{+}\rangle$ state preparation protocol fidelity for the same noise parameters as in (c).

Moreover, keeping the SCSs close to the equatorial plane makes them also robust against dephasing. This is evident from the differential of the diagonal matrix elements in the logical qubit subspace [41],

$$\langle\theta_1,\varphi_1|(\hat{F}_{g,z})^{n_z}|\theta_1,\varphi_1\rangle - \langle\theta_2,\varphi_2|(\hat{F}_{g,z})^{n_z}|\theta_2,\varphi_2\rangle = 2(F_g\cos\theta_1)^{n_z} + \cos\theta_1\mathcal{O}(F_g^{n_z-1}), \tag{4}$$

for orthogonal SCS $(\theta_2,\varphi_2) = (\pi - \theta_1, \pi + \varphi_1)$, which vanishes for $\theta_1 = \pi/2$.

Autonomous stabilization—Another type of error that can occur is leakage from the logical qubit space. Such leakage errors can be converted primarily into dephasing errors by combining laser driving and spontaneous emission. It is useful to first consider a frame transformation, by rotating the quantization axis to that determined by $\mathbf{\Omega}$; see Supplemental Material [46]. In this frame, the laser drive is linearly polarized, coupling only the interior levels ($|m| < F_g$) to the F_e manifold; see Fig. 3(a). In this eigenbasis, the DSs are the two maximally stretched spin states of the F_g manifold, separated by $2F_g - 1$ pairs of bright states. Noise processes associated to $(\hat{F}_{z,g})^{n_z}$, with $n_z \ll F_g$, couple the DSs to the interior bright states. This leakage is determined by the noise strength relative to the

gap from the dark to the relevant bright state and, thus, can be minimized by increasing $|\mathbf{\Omega}|$.

Importantly, spontaneous emission, of strength γ, from the F_e component of the bright states favors decay processes toward the closest DS due to the associated CG coefficients [47], effectively driving leaked population directly back to the qubit state it originated from, converting the error into dephasing. Hence, the combined action of the laser driving and spontaneous emission is a BP stabilization process, in analogy to bosonic systems [57]. The timescale of autonomous stabilization is in the limit $|\mathbf{\Omega}| \gg \gamma$ determined by $\gamma/(2F_g+1)$ as discussed in Supplemental Material [46]. Autonomous stabilization is particularly suited to broad $F \leftrightarrow F-1$ laser-cooling transitions, with $F \gg 1$, e.g., the ground state of Nd or metastable excited states of Dy [58]. Further, the amplitude error mentioned in [39] can be corrected passively given that we can engineer specific polarizations of the emission [59]; see Supplemental Material [46].

Colored noise—We now analyze the robustness of the dark spin cat subjected to colored Markovian noise processes $X(t)$, governed by an Ornstein-Uhlenbeck process, with correlation time $1/\lambda$ and diffusion constant $\lambda^2\kappa/2$, coupling to $\hat{F}_{g,z}$, e.g., a fluctuating magnetic field. Note, κ is the noise strength in the white noise limit $\lambda/|\mathbf{\Omega}| \to \infty$ [60]. Following Miao [61], we directly compute the stochastic average of the system state $\hat{\rho}(t)$ over all possible noise trajectories [46,62,63]. The resulting error channel can be characterized by the Pauli transfer matrix (PTM) [64,65],

$$R_{n,m}(t) = \mathrm{tr}[\hat{E}_n \hat{\rho}_m(t)]/2 \quad \text{for } \hat{\rho}_m(0) = \hat{E}_m, \tag{5}$$

with $\hat{E}_n \in \{\tilde{\mathbb{1}}, \hat{\sigma}_{\tilde{x}}, \hat{\sigma}_{\tilde{y}}, \hat{\sigma}_{\tilde{z}}\}$, where $\tilde{\mathbb{1}}$ denotes the qubit subspace projector. The diagonal elements of $\mathbf{R}(t)$ carry the relevant error channel information [66,67], where $R_{\tilde{x},\tilde{x}}(t) = R_{\tilde{y},\tilde{y}}(t)$ and $R_{\tilde{z},\tilde{z}}(t)$ are associated with the dephasing and bit-flip error, respectively; see Supplemental Material [46].

In Figs. 1(c) and 3(b) we present the diagonal elements of $\mathbf{R}(t)$ for dark spin-cat qubits subjected to colored noise, exhibiting a suppression of both bit-flip and dephasing errors by increasing laser coupling strength. Bit-flip error rates decrease exponentially in F_g, while phase-flip errors increase only polynomially. Note, in Fig. 1(c), the same parameters as in Fig. 3(b) are used. Typical values of $\mathbf{\Omega}$ for electric dipole transitions are several hundred MHz, for which we observe a severe reduction of effective noise rates, even for very strong noise with $\kappa, \lambda \sim O(10\text{–}100\ \mathrm{kHz})$. The overall strength of the error rates is determined by the power spectral density at the gap frequency $\propto |\mathbf{\Omega}|$. For $\lambda \gtrsim |\mathbf{\Omega}|$, the noise becomes white and is described by Lindbladian dynamics with jump operator $\sqrt{\kappa}\hat{F}_{g,z}$ [see Fig. 3(b)], for which we still observe an exponential bias [46].

Logical operations—We now discuss error channels of single-qubit gates in the presence of colored noise processes as discussed above. In Fig. 3(c) we present for $\hat{U}_{\tilde{z}}(\alpha)$ the diagonal elements of $\mathbf{R}(T)$ adjusted by the inverse error-free unitary gate. The worst-case gate infidelity is, due to the biasedness of the channel $1-R_{\tilde{z},\tilde{z}}(T) \ll 1-R_{\tilde{x},\tilde{x}}(T)$, given by $1-\mathcal{F} = [1-R_{\tilde{x},\tilde{x}}(T)]/2$ [68]. At small T, the gate fidelity is limited by adiabaticity violations, while at large T the noise $X(t)$ is the limiting factor. The former can be mitigated with counterdiabatic driving techniques [46,69]. Nevertheless, for $|\mathbf{\Omega}| = 2\pi \times 300$ MHz, the gate can be executed as fast as $T = 1\ \mu\mathrm{s}$ in a bias preserving manner, with an infidelity below 10^{-2}. We note that $\hat{U}_{\tilde{x}}$ can be performed *virtually*, with perfect fidelity, by swapping definitions of $|\tilde{0}\rangle$ and $|\tilde{1}\rangle$.

Initialization—Preparation of a logical state, such as $|\widetilde{+}\rangle = (|\tilde{0}\rangle + |\tilde{1}\rangle)/\sqrt{2}$, can be accomplished by first preparing the qubit in the stretched state $|F_g, -F_g\rangle$ (for $\Omega^{-1} > 0$) using optical pumping. This state is then adiabatically converted by first ramping on Ω^{+1}, akin to a STIRAP protocol [70] (see Supplemental Material [46]). The corresponding fidelity, i.e., overlap, is presented in Fig. 3(d). Measurement can be performed by reversing the preparation method and subsequently monitoring the population of $|F_g, -F_g\rangle$.

Entangling gates—A universal set of quantum gates requires the implementation of an entangling operation, which we exemplify here for neutral atoms laser excited to Ry states. We consider dark spin-cat qubits encoded in the maximally stretched HF manifold of the metastable $^3P_2$ [71] fine structure manifold of fermionic divalent atoms, such as ^{171}Yb, ^{173}Yb or ^{87}Sr, for which $F_g = 5/2, 9/2, 13/2$, respectively. Autonomous stabilization is achieved by coupling to the maximally stretched lowest $^3S_1$ manifold [72].

To harness full advantage of the dark spin cat's biased noise structure, BP operations have to be employed. First, we outline the implementation of a $\hat{\mathrm{C}}_Z$ gate. For this, the control and target atom are rotated to SCS pointing along the z axis enabling selective excitation to a maximally stretched $^3S_1$ ($F_r = F_g - 1$) Ry state [73] [see Fig. 4(a)], which allows for the execution of state-of-the-art $\hat{\mathrm{C}}_Z$ gates [33,74,75]. Additionally, neutral atom platforms are amenable to erasure conversion techniques [17,33]. Especially, $^3P_2$ dark spin-cat encoding offers the possibility to pump leaked population to $^1S_0$ from where it can be detected [76,77]. For the $\hat{\mathrm{C}}_Z$ gate, only one of the two qubit states is Ry excited. Leakage due to spontaneous emission thus originates predominantly only from one of the qubit states, enabling high-threshold QEC strategies based on *biased* erasure [78]. Further, Ry decay events that return to the encoded F_g manifold, which cannot be converted to erasure, do not introduce bit-flip errors due to the

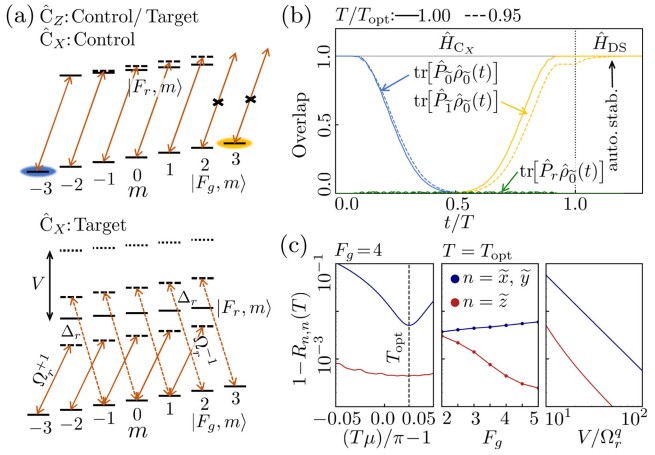

FIG. 4. Entangling gates: (a) $\hat{C}_Z$ and $\hat{C}_X$ laser coupling scheme to Ry states for $F_g = 3$. For the $\hat{C}_Z$ gate execution the target and control atom are encoded along the z axis, while for the $\hat{C}_X$ gate the control atom is encoded along the z axis and the target atom along the x axis. (b) $\hat{C}_X$: time evolution of the target atom starting from $|\tilde{0}\rangle$, when the control atom is not Ry excited, for two different gate times. $\hat{P}_{\tilde{0}}$, $\hat{P}_{\tilde{1}}$, $\hat{P}_r$ denote projectors onto $|\tilde{0}\rangle$, $|\tilde{1}\rangle$ and all $|F_r, m\rangle$ states, respectively. Here, and in all remaining panels, $F_g = 4$, $\Omega_r^q/\Delta_r = 1/2$, $\Omega_r^q = 2\pi \times 3$ MHz, and $\delta_r = 0$ if not stated otherwise. (c) $\hat{C}_X$: diagonal elements of $\mathbf{R}(T)$ for different gate times (left), at the optimal gate time $T_{\rm opt}$ for different F_g (middle) and when the control atom is Ry excited for different V (right).

separation of magnetic quanta and the autonomous stabilization. This is in contrast to the existing protocols [17,78] where no Pauli error bias exists when the population decays back to the encoded subspace. Thus, dark spin-cat encoding naturally realizes biased erasure conversion alongside a more structured error model, which has the potential to further enhance the error threshold.

The $\hat{C}_Z$ gate, together with 1-qubit $\hat{U}_{\tilde{z}}(\alpha_z)$ and $\hat{U}_{\tilde{x}}(\alpha_x)$ rotations, forms a universal gate set. Detailed information on $\hat{U}_{\tilde{x}}(\alpha_x)$ is provided in Supplemental Material [46]. However, other entangling operations like a $\hat{C}_X$ (CNOT) gate implemented in this manner do not preserve Pauli error bias. The direct execution of BP $\hat{C}_X$ and $\widehat{CC}_X$ (Toffoli) gates is required for a full BP operation set that leads to universal computing on the logical level [11] and usually results in a higher threshold compared with the non-BP implementation of those operations [20,78]. We provide a detailed protocol for a BP $\hat{C}_X$ gate in the following. The implementation is based on an artificial local magnetic field $\mu\hat{F}_z$ (μ is the field strength), engineered through light-induced AC Stark shifts [54,79], exchanging the qubit states of the target atom. Its action can be made conditional on the state of the control atom by means of the Ry blockade effect [80,81]. The target qubit is encoded in SCSs along the x axis with the stabilization turned off during the gate. The artificial magnetic field responsible for exchanging the qubit states is implemented by off-resonantly coupling the states $|F_g, m\rangle$ by two circularly polarised laser fields to the Ry states mentioned for $\hat{C}_Z$ labeled by $|F_r, m\rangle$. The corresponding Hamiltonian is given by Eq. (1), but with the replacement $e \leftrightarrow r$, $\Delta = 0$, and not on Raman resonance, i.e., with couplings $\Omega_r^q \hat{C}_q \exp(iq\Delta_r)$; see Fig. 4(a). In the limit $|\Omega_r^{+1}| = |\Omega_r^{-1}| \ll |\Delta_r|$, the laser coupling gives rise to an artificial magnetic field with strength $\mu = (|\Omega_r^q|^2/4\Delta_r)(1/F_g)[(2F_g - 1)/(2F_g + 1)]$ up to second order in Ω_r^q/Δ_r.

Similar to the $\hat{C}_Z$ gate the control atom is rotated to the z axis from where state selective Ry excitation is possible [Fig. 4(a)]. Notably, the transformation to the z axis is achieved by rotating the SCSs around the y axis, which is in analogy to $\hat{U}_{\tilde{x}}$ a BP process. If excited, the control atom shifts the energies of the target atom due to van der Waals interactions [73], with an interaction shift $V \gg \Delta_r$, rendering the artificial magnetic field inoperative. The resulting Hamiltonian reads $\hat{H}_{C_X} = (\mathbb{1} - \hat{P}_r) \otimes \mu\hat{F}_{z,g}$ up to second order in Ω_r^q/Δ_r and first order in Ω_r^q/V, where $\hat{P}_r$ denotes the Ry state projector. The desired entangling gate is then effected by $\hat{C}_X = \exp(-i\hat{H}_{C_X}T)$, where $T \sim \pi/\mu$ is the gate time obtained from numerical simulations. Furthermore, we consider different Ry states or even different species for the control and target atoms in order to mitigate crosstalk [46].

In Fig. 4(b) we present the time evolution of the target atom if the control atom is not Ry excited, demonstrating a swap of the qubit states. We also analyze a deliberate underrotation, inducing leakage from the qubit subspace. This population can be repumped by turning on the autonomous stabilization, $\hat{H}_{DS}$ from Eq. (1). Overall, this leads to a bias preserving gate, even in the presence of over- or underrotation errors [see left and middle panel Fig. 4(c)].

In the middle panel of Fig. 4(c) we present dephasing and bit-flip errors when the control atom is Ry excited. The bit-flip error is exponentially suppressed in F_g as compared to the dephasing error. Deviations from exponential suppression for large F_g are due to higher order corrections and can be reduced by decreasing Ω_r^q/Δ_r. In the right panel of Fig. 4(c) we show the same errors as a function of the Rydberg blockade strength V. The overall worst-case gate infidelity $1 - \mathcal{F} = [1 - R_{\tilde{x},\tilde{x}}(T)]/2$ (as discussed above) can be on the order of 10^{-3}, with $\Omega_r^q = 2\pi \times 3$ MHz, $\Delta_r = 2\pi \times 6$ MHz resulting in $T_{\rm opt} = 8.5$ μs requiring $V \sim 2\pi \times O(100\ \text{MHz})$ for $F_g = 4$.

The proposed implementation of a BP $\hat{C}_X$ gate comes at the cost of an increased implementation complexity as compared to state-of-the-art $\hat{C}_Z$ gates. Specifically, comparably long gate times can render decay of the Ry excited control atom relevant, leading to nonbias preserving processes. However, this decay could, for example, be mitigated by multiplying the number of control atoms [82] or by

detecting the decay of a control atom using erasure conversion [33]. A thorough analysis incorporating control atom decay and its mitigation is presented in the SM [46]. While initial experimental implementations of the BP $\hat{C}_X$ gate would likely struggle to achieve fidelities similar to existing state-of-the-art $\hat{C}_Z$ gates, the additional structure in the error model in turn would lead to higher error thresholds [20,78,83]. Investigating this trade-off could be an interesting avenue for further study. Finally, we note that the approach presented is highly modular, e.g., a $\widehat{CC}_X$ gate can be constructed by separately exciting two control atoms instead of one.

Conclusions—We introduced an atomic dark spin-cat qubit encoding featuring a BP error model and autonomous stabilization. We provide proof-of-principle gate implementations on a Ry platform but emphasize that all results can not only be improved significantly using optimal control techniques or counteradiabatic driving [69,84] but also directly extended to other platforms such as trapped ions [42]. In particular, the single qubit control can be extended to trapped ions and an entangling gate is realizable by rotating the qubits to the z axis from where the geometric phase entangling gate [85] is executable; however, we reserve detailed analysis for future work. The encoding scheme could also benefit quantum simulations with magnetic atoms ^{167}Er or ^{161}Dy and heteronuclear molecules ^{40}K^{87}Rb, engineering a closed qubit subspace with strong and tunable dipolar interactions [86,87]. Higher order multipole couplings enable the construction of "multilegged" spin cats, offering the possibility to redundantly encode quantum information in a single atom in order to tolerate more errors while preserving large error bias [8,88]. Overall, spin-cat encodings with biased error models implemented in single atoms could provide a viable platform enabling resource-efficient quantum error correction codes, meeting the demanding requirements of fault-tolerant quantum computation.

Note added—During the submission process, we became aware of several experimental advances closely related to our protocols, including spin-cat state preparation [89] and the use of spin-cat states for measurement-free (autonomous) error correction against dephasing noise in a single ion [90,91].

Acknowledgments—We would like to thank J. Zeiher, M. Ammenwerth, G. Giudice, A. Retzker, I. Deutsch, M. Lukin, A. Kaufman, J. Ye, and A. M. Rey for enlightening discussions. This work was supported by the European High-Performance Computing Joint Undertaking (JU) under Grant No. 101018180 HPCQS, the Horizon Europe programme HORIZON-CL4-2022-QUANTUM-02-SGA via the Project 101113690 (PASQuanS2.1), the ARO (W911NF-23-1-0077), ARO MURI (W911NF-21-1-0325), AFOSR MURI (FA9550-19-1-0399, FA9550-21-1-0209, FA9550-23-1-0338), DARPA (HR0011-24-9-0359, HR0011-24-9-0361), NSF (OMA-1936118, ERC-1941583, OMA-2137642, OSI-2326767, CCF-2312755), NTT Research, Samsung GRO, Packard Foundation (2020-71479).

[1] P. Shor, Fault-tolerant quantum computation, *Proceedings of 37th conference on foundations of computer science* (IEEE, 1996).
[2] A. M. Steane, Efficient fault-tolerant quantum computing, Nature (London) **399**, 124 (1999).
[3] A. G. Fowler, M. Mariantoni, J. M. Martinis, and A. N. Cleland, Surface codes: Towards practical large-scale quantum computation, Phys. Rev. A **86**, 032324 (2012).
[4] D. Gottesman, Fault-tolerant quantum computation with constant overhead, arXiv:1310.2984.
[5] E. T. Campbell, B. M. Terhal, and C. Vuillot, Roads towards fault-tolerant universal quantum computation, Nature (London) **549**, 172 (2017).
[6] D. Gottesman, Opportunities and challenges in fault-tolerant quantum computation, arXiv:2210.15844.
[7] D. Gottesman, A. Kitaev, and J. Preskill, Encoding a qubit in an oscillator, Phys. Rev. A **64**, 012310 (2001).
[8] M. Mirrahimi, Z. Leghtas, V. V. Albert, S. Touzard, R. J. Schoelkopf, L. Jiang, and M. H. Devoret, Dynamically protected cat-qubits: A new paradigm for universal quantum computation, New J. Phys. **16**, 045014 (2014).
[9] M. H. Michael, M. Silveri, R. T. Brierley, V. V. Albert, J. Salmilehto, L. Jiang, and S. M. Girvin, New class of quantum error-correcting codes for a bosonic mode, Phys. Rev. X **6**, 031006 (2016).
[10] P. Aliferis and J. Preskill, Fault-tolerant quantum computation against biased noise, Phys. Rev. A **78**, 052331 (2008).
[11] J. Guillaud and M. Mirrahimi, Repetition cat qubits for fault-tolerant quantum computation, Phys. Rev. X **9**, 041053 (2019).
[12] S. Puri, L. St-Jean, J. A. Gross, A. Grimm, N. E. Frattini, P. S. Iyer, A. Krishna, S. Touzard, L. Jiang, A. Blais *et al.*, Bias-preserving gates with stabilized cat qubits, Sci. Adv. **6** (2020).
[13] C. Chamberland, K. Noh, P. Arrangoiz-Arriola, E. T. Campbell, C. T. Hann, J. Iverson, H. Putterman, T. C. Bohdanowicz, S. T. Flammia, A. Keller, G. Refael, J. Preskill, L. Jiang, A. H. Safavi-Naeini, O. Painter, and F. G. S. L. Brandão, Building a fault-tolerant quantum computer using concatenated cat codes, PRX Quantum **3**, 010329 (2022).
[14] V. V. Albert, S. O. Mundhada, A. Grimm, S. Touzard, M. H. Devoret, and L. Jiang, Pair-cat codes: Autonomous error-correction with low-order nonlinearity, Quantum Sci. Technol. **4**, 035007 (2019).
[15] M. Yuan, Q. Xu, and L. Jiang, Construction of bias-preserving operations for pair-cat codes, Phys. Rev. A **106**, 062422 (2022).
[16] J. D. Teoh, P. Winkel, H. K. Babla, B. J. Chapman, J. Claes, S. J. de Graaf, J. W. Garmon, W. D. Kalfus, Y. Lu, A. Maiti *et al.*, Dual-rail encoding with superconducting cavities, Proc. Natl. Acad. Sci. U.S.A. **120** (2023).
[17] Y. Wu, S. Kolkowitz, S. Puri, and J. D. Thompson, Erasure conversion for fault-tolerant quantum computing

in alkaline earth Rydberg atom arrays, Nat. Commun. **13**, 4657 (2022).
[18] A. Kubica, A. Haim, Y. Vaknin, H. Levine, F. Brandão, and A. Retzker, Erasure qubits: Overcoming the T1 limit in superconducting circuits, Phys. Rev. X **13**, 041022 (2023).
[19] D. K. Tuckett, S. D. Bartlett, and S. T. Flammia, Ultrahigh error threshold for surface codes with biased noise, Phys. Rev. Lett. **120**, 050505 (2018).
[20] A. S. Darmawan, B. J. Brown, A. L. Grimsmo, D. K. Tuckett, and S. Puri, Practical quantum error correction with the XZZX code and Kerr-cat qubits, PRX Quantum **2**, 030345 (2021).
[21] P. Scholl, M. Schuler, H. J. Williams, A. A. Eberharter, D. Barredo, K.-N. Schymik, V. Lienhard, L.-P. Henry, T. C. Lang, T. Lahaye *et al.*, Quantum simulation of 2d antiferromagnets with hundreds of Rydberg atoms, Nature (London) **595**, 233 (2021).
[22] A. J. Park, J. Trautmann, N. Šantić, V. Klüsener, A. Heinz, I. Bloch, and S. Blatt, Cavity-enhanced optical lattices for scaling neutral atom quantum technologies to higher qubit numbers, PRX Quantum **3**, 030314 (2022).
[23] S. Ebadi, T. T. Wang, H. Levine, A. Keesling, G. Semeghini, A. Omran, D. Bluvstein, R. Samajdar, H. Pichler, W. W. Ho *et al.*, Quantum phases of matter on a 256-atom programmable quantum simulator, Nature (London) **595**, 227 (2021).
[24] D. Kiesenhofer, H. Hainzer, A. Zhdanov, P. C. Holz, M. Bock, T. Ollikainen, and C. F. Roos, Controlling two-dimensional Coulomb crystals of more than 100 ions in a monolithic radio-frequency trap, PRX Quantum **4**, 020317 (2023).
[25] H. J. Manetsch, G. Nomura, E. Bataille, K. H. Leung, X. Lv, and M. Endres, A tweezer array with 6100 highly coherent atomic qubits, arXiv:2403.12021.
[26] J. P. Gaebler, T. R. Tan, Y. Lin, Y. Wan, R. Bowler, A. C. Keith, S. Glancy, K. Coakley, E. Knill, D. Leibfried *et al.*, High-fidelity universal gate set for $^{9}Be^{+}$ ion qubits, Phys. Rev. Lett. **117**, 060505 (2016).
[27] R. Finkelstein, R. Tsai, X. Sun, P. Scholl, S. Direkci, T. Gefen, J. Choi, A. Shaw, and M. Endres, Universal quantum operations and ancilla-based readout for tweezer clocks, Nature (London) **634**, 321 (2024).
[28] S. Anand, C. E. Bradley, R. White, V. Ramesh, K. Singh, and H. Bernien, A dual-species Rydberg array, Nat. Phys. **20**, 1744 (2024).
[29] M. Peper, Y. Li, D. Y. Knapp, M. Bileska, S. Ma, G. Liu, P. Peng, B. Zhang, S. P. Horvath, A. P. Burgers *et al.*, Spectroscopy and Modeling of 171Yb Rydberg States for High-Fidelity Two-Qubit Gates, Phys. Rev. X **15**, 011009 (2025).
[30] K. Wright, K. M. Beck, S. Debnath, J. Amini, Y. Nam, N. Grzesiak, J.-S. Chen, N. Pisenti, M. Chmielewski, C. Collins *et al.*, Benchmarking an 11-qubit quantum computer, Nat. Commun. **10**, 5464 (2019).
[31] C. J. Ballance, T. P. Harty, N. M. Linke, M. A. Sepiol, and D. M. Lucas, High-fidelity quantum logic gates using trapped-ion hyperfine qubits, Phys. Rev. Lett. **117**, 060504 (2016).
[32] C. R. Clark, H. N. Tinkey, B. C. Sawyer, A. M. Meier, K. A. Burkhardt, C. M. Seck, C. M. Shappert, N. D. Guise, C. E. Volin, S. D. Fallek *et al.*, High-fidelity Bell-state preparation with $^{40}Ca^{+}$ optical qubits, Phys. Rev. Lett. **127**, 130505 (2021).
[33] S. Ma, G. Liu, P. Peng, B. Zhang, S. Jandura, J. Claes, A. P. Burgers, G. Pupillo, S. Puri, and J. D. Thompson, High-fidelity gates and mid-circuit erasure conversion in an atomic qubit, Nature (London) **622**, 279 (2023).
[34] H. Levine, A. Keesling, G. Semeghini, A. Omran, T. T. Wang, S. Ebadi, H. Bernien, M. Greiner, V. Vuletić, H. Pichler *et al.*, Parallel implementation of high-fidelity multiqubit gates with neutral atoms, Phys. Rev. Lett. **123**, 170503 (2019).
[35] A. Sørensen and K. Mølmer, Quantum computation with ions in thermal motion, Phys. Rev. Lett. **82**, 1971 (1999).
[36] R. B.-S. Tsai, X. Sun, A. L. Shaw, R. Finkelstein, and M. Endres, Benchmarking and linear response modeling of high-fidelity Rydberg gates, PRX Quantum **6**, 010331 (2025).
[37] I. Pogorelov, F. Butt, L. Postler, C. D. Marciniak, P. Schindler, M. Müller, and T. Monz, Experimental fault-tolerant code switching, arXiv:2403.13732.
[38] D. Bluvstein, S. J. Evered, A. A. Geim, S. H. Li, H. Zhou, T. Manovitz, S. Ebadi, M. Cain, M. Kalinowski, D. Hangleiter *et al.*, Logical quantum processor based on reconfigurable atom arrays, Nature (London) **626**, 58 (2024).
[39] S. Omanakuttan, V. Buchemmavari, J. A. Gross, I. H. Deutsch, and M. Marvian, Fault-tolerant quantum computation using large spin-cat codes, PRX Quantum **5**, 020355 (2024).
[40] N. Timoney, I. Baumgart, M. Johanning, A. Varón, M. B. Plenio, A. Retzker, and C. Wunderlich, Quantum gates and memory using microwave-dressed states, Nature (London) **476**, 185 (2011).
[41] N. Aharon, M. Drewsen, and A. Retzker, General scheme for the construction of a protected qubit subspace, Phys. Rev. Lett. **111**, 230507 (2013).
[42] G. Mikelsons, I. Cohen, A. Retzker, and M. B. Plenio, Universal set of gates for microwave dressed-state quantum computing, New J. Phys. **17**, 053032 (2015).
[43] S. Weidt, J. Randall, S. C. Webster, K. Lake, A. E. Webb, I. Cohen, T. Navickas, B. Lekitsch, A. Retzker, and W. K. Hensinger, Trapped-ion quantum logic with global radiation fields, Phys. Rev. Lett. **117**, 220501 (2016).
[44] N. Aharon, M. Drewsen, and A. Retzker, Enhanced quantum sensing with multi-level structures of trapped ions, Quantum Sci. Technol. **2**, 034006 (2017).
[45] Microwave radiation acts globally on the atom ensemble and, thus, lacks single site addressability. Single-site resolution can be restored using additional laser-driving fields. For simplicity we focus here on laser light.
[46] See Supplemental Material at http://link.aps.org/supplemental/10.1103/w9zh-jwsx for detailed discussions on spin coherent states, biased-noise analysis, gate operations, and numerical simulations.
[47] I. I. Sobelman, *Introduction to the Theory of Atomic Spectra*, International Series of Monographs in Natural Philosophy Vol. 40 (Elsevier, New York, 2016).
[48] J. R. Morris and B. W. Shore, Reduction of degenerate two-level excitation to independent two-state systems, Phys. Rev. A **27**, 906 (1983).

[49] P. Zanardi and M. Rasetti, Holonomic quantum computation, Phys. Lett. A **264**, 94 (1999).

[50] A. Recati, T. Calarco, P. Zanardi, J. I. Cirac, and P. Zoller, Holonomic quantum computation with neutral atoms, Phys. Rev. A **66**, 032309 (2002).

[51] V. V. Albert, C. Shu, S. Krastanov, C. Shen, R.-B. Liu, Z.-B. Yang, R. J. Schoelkopf, M. Mirrahimi, M. H. Devoret, and L. Jiang, Holonomic quantum control with continuous variable systems, Phys. Rev. Lett. **116**, 140502 (2016).

[52] C.-F. Kam, W.-M. Zhang, D.-H. Feng *et al.*, *Coherent States: New Insights into Quantum Mechanics with Applications* (Springer, New York, 2023).

[53] Additionally, imperfect laser polarization gives rise to AC-Stark shifts, altering the energy and the composition of the DSs. These effects are rendered negligible by the applied magnetic field [41].

[54] F. Le Kien, P. Schneeweiss, and A. Rauschenbeutel, Dynamical polarizability of atoms in arbitrary light fields: General theory and application to cesium, Eur. Phys. J. D **67**, 92 (2013).

[55] J. D. Thompson, T. G. Tiecke, A. S. Zibrov, V. Vuletić, and M. D. Lukin, Coherence and Raman sideband cooling of a single atom in an optical tweezer, Phys. Rev. Lett. **110**, 133001 (2013).

[56] Noise operators in the rotating frame: The diagonal components $\hat{\mathcal{U}}(\hat{F}_{g,z})^n\hat{\mathcal{U}}^\dagger = (\hat{F}_{g,z})^n$ are invariant under the rotating frame transformation. The off-diagonal components $\hat{\mathcal{U}}\hat{F}_{g,\pm}\hat{\mathcal{U}}^\dagger = \exp(\pm i\delta_g t)\hat{F}_{g,\pm}$ become oscillatory in time, with $\hat{F}_{g,\pm} = \hat{F}_{g,x} \pm i\hat{F}_{g,y}$. Thus, off-diagonal noise components average out as long as the corresponding noise amplitude and time dependency is much smaller (slower) than $|\mathbf{\Omega}|$. Note, for polynomials of spin operators, as considered in the main text, similar identities can be derived.

[57] J. Guillaud, J. Cohen, and M. Mirrahimi, Quantum computation with cat qubits, SciPost Phys. Lect. Notes 072 (2023).

[58] G. Hovhannesyan and M. Lepers, Improving the spectroscopic knowledge of neutral neodymium, Phys. Scr. **98**, 025407 (2023).

[59] A. Piñeiro Orioli, J. K. Thompson, and A. M. Rey, Emergent dark states from superradiant dynamics in multilevel atoms in a cavity, Phys. Rev. X **12**, 011054 (2022).

[60] C. Gardiner, *Stochastic Methods* (Springer, Berlin, 2009), Vol. 4.

[61] D. W.-C. Miao, Analysis of the discrete Ornstein-Uhlenbeck process caused by the tick size effect, Appl. Probab. **50**, 1102 (2013).

[62] N. G. Van Kampen, Stochastic differential equations, Phys. Rep. **24**, 171 (1976).

[63] P. Zoller, G. Alber, and R. Salvador, AC Stark splitting in intense stochastic driving fields with Gaussian statistics and non-Lorentzian line shape, Phys. Rev. A **24**, 398 (1981).

[64] M. A. Nielsen and I. L. Chuang, *Quantum Computation and Quantum Information* (Cambridge University Press, Cambridge, England, 2010).

[65] D. Greenbaum, Introduction to quantum gate set tomography, arXiv:1509.02921.

[66] A. Erhard, J. J. Wallman, L. Postler, M. Meth, R. Stricker, E. A. Martinez, P. Schindler, T. Monz, J. Emerson, and R. Blatt, Characterizing large-scale quantum computers via cycle benchmarking, Nat. Commun. **10**, 5347 (2019).

[67] E. Magesan, J. M. Gambetta, and J. Emerson, Scalable and robust randomized benchmarking of quantum processes, Phys. Rev. Lett. **106**, 180504 (2011).

[68] States most sensitive to dephasing are on the equator of the logical qubit Bloch-sphere. The worst case fidelity is obtained by uniformly sampling over these states.

[69] A. del Campo, Shortcuts to adiabaticity by counterdiabatic driving, Phys. Rev. Lett. **111**, 100502 (2013).

[70] N. V. Vitanov, A. A. Rangelov, B. W. Shore, and K. Bergmann, Stimulated Raman adiabatic passage in physics, chemistry, and beyond, Rev. Mod. Phys. **89**, 015006 (2017).

[71] V. Klüener, S. Pucher, D. Yankelev, J. Trautmann, F. Spriestersbach, D. Filin, S. G. Porsev, M. S. Safronova, I. Bloch, and S. Blatt, Lived Coherence on a μhz Scale Optical Magnetic Quadrupole Transition, Phys. Rev. Lett. **132**, 253201 (2024).

[72] We note that this transition is only partially cyclic; thus, spontaneous emission leads to decay outside the F_g manifold, requiring a suitable choice of repumping lasers.

[73] F. Robicheaux, Calculations of long range interactions for 87Sr Rydberg states, J. Phys. B **52**, 244001 (2019).

[74] S. J. Evered, D. Bluvstein, M. Kalinowski, S. Ebadi, T. Manovitz, H. Zhou, S. H. Li, A. A. Geim, T. T. Wang, N. Maskara *et al.*, High-fidelity parallel entangling gates on a neutral-atom quantum computer, Nature (London) **622**, 268 (2023).

[75] A. Cao, W. J. Eckner, T. Lukin Yelin, A. W. Young, S. Jandura, L. Yan, K. Kim, G. Pupillo, J. Ye, N. Darkwah Oppong *et al.*, Multi-qubit gates and Schrödinger cat states in an optical clock, Nature (London) **634**, 315 (2024).

[76] R. Yamamoto, J. Kobayashi, T. Kuno, K. Kato, and Y. Takahashi, An ytterbium quantum gas microscope with narrow-line laser cooling, New J. Phys. **18**, 023016 (2016).

[77] S. Saskin, J. T. Wilson, B. Grinkemeyer, and J. D. Thompson, Narrow-line cooling and imaging of ytterbium atoms in an optical tweezer array, Phys. Rev. Lett. **122**, 143002 (2019).

[78] K. Sahay, J. Jin, J. Claes, J. D. Thompson, and S. Puri, High-threshold codes for neutral-atom qubits with biased erasure errors, Phys. Rev. X **13**, 041013 (2023).

[79] C. Cohen-Tannoudji and J. Dupont-Roc, Experimental study of Zeeman light shifts in weak magnetic fields, Phys. Rev. A **5**, 968 (1972).

[80] D. Jaksch, J. I. Cirac, P. Zoller, S. L. Rolston, R. Côté, and M. D. Lukin, Fast quantum gates for neutral atoms, Phys. Rev. Lett. **85**, 2208 (2000).

[81] M. D. Lukin, M. Fleischhauer, R. Cote, L. M. Duan, D. Jaksch, J. I. Cirac, and P. Zoller, Dipole blockade and quantum information processing in mesoscopic atomic ensembles, Phys. Rev. Lett. **87**, 037901 (2001).

[82] I. Cong, H. Levine, A. Keesling, D. Bluvstein, S.-T. Wang, and M. D. Lukin, Hardware-efficient, fault-tolerant quantum computation with Rydberg atoms, Phys. Rev. X **12**, 021049 (2022).

[83] G. Baranes, M. Cain, J. P. B. Ataides, D. Bluvstein, J. Sinclair, V. Vuletic, H. Zhou, and M. D. Lukin, Leveraging atom loss errors in fault tolerant quantum algorithms, arXiv:2502.20558.

[84] M. V. Berry, Transitionless quantum driving, J. Phys. A **42**, 365303 (2009).
[85] D. Leibfried, B. DeMarco, V. Meyer, D. Lucas, M. Barrett, J. Britton, W. M. Itano, B. Jelenković, C. Langer, T. Rosenband *et al.*, Experimental demonstration of a robust, high-fidelity geometric two ion-qubit phase gate, Nature (London) **422**, 412 (2003).
[86] M. A. Perlin, D. Barberena, M. Mamaev, B. Sundar, R. J. Lewis-Swan, and A. M. Rey, Engineering infinite-range SU(n) interactions with spin-orbit-coupled fermions in an optical lattice, Phys. Rev. A **105**, 023326 (2022).
[87] A. Kruckenhauser, L. M. Sieberer, L. De Marco, J.-R. Li, K. Matsuda, W. G. Tobias, G. Valtolina, J. Ye, A. M. Rey, M. A. Baranov *et al.*, Quantum many-body physics with ultracold polar molecules: Nanostructured potential barriers and interactions, Phys. Rev. A **102**, 023320 (2020).
[88] Z. Leghtas, G. Kirchmair, B. Vlastakis, R. J. Schoelkopf, M. H. Devoret, and M. Mirrahimi, Hardware-efficient autonomous quantum memory protection, Phys. Rev. Lett. **111**, 120501 (2013).
[89] Y. A. Yang, W.-T. Luo, J.-L. Zhang, S.-Z. Wang, Chang-Ling Zou, T. Xia, and Z.-T. Lu, Minute-scale Schrödinger-cat state of spin-5/2 atoms, Nat. Photon. **19**, 85 (2025).
[90] K. DeBry, N. Meister, A. V. Martinez *et al.*, Error correction of a logical qubit encoded in a single atomic ion, arXiv:2503.13908.
[91] Y. Li, Q. Mei, Q.-X. Jie *et al.*, Beating the break-even point with autonomous quantum error correction, arXiv:2504.16746.